AN ABSTRACT OF THE PAPER OF

Nolan E. Mitchell for the degree of Master of Arts in Applied Mathematics
presented on
Title: Multi-Dimensional Sampling in Fan Beam Tomography

In this paper we explore a new sampling scheme proposed by S. H. Izen, D. P. Rohler, and K.L.A. Sastry [4] for fan beam tomography. This method exploits the reflection property of the fan beam transform via multi-dimensional sampling theory and is more efficient than the standard scheme in the sense that half as many measurements are needed to obtain the same resolution. We depart from the work of Izen et al. by employing Faridani's generalized sampling expansion [5] [7].

Multi-Dimensional Sampling in Fan Beam Tomography

by
Nolan E. Mitchell

submitted to

Oregon State University

in partial fulfillment of
the requirements for the
degree of

Master of Arts

TABLE OF CONTENTS

LIST OF FIGURES

Figure 1: *The Siemens SOMATOM Sensation 64 CT scanner. This scanner can measure 64 fans simultaneously with a gantry rotation speed of 0.33 seconds. Image courtesy of Siemens Medical Solutions [23].*

1 Introduction

The goal of computed tomography (CT) is to create an accurate image of the interior of an object in a nondestructive way. One well-known example is the use of x-ray CT in medical scans, sometimes called CAT (computerized axial tomography) scans. In this paper we will be concerned with the so-called third generation of medical CT scanners (see Figure 1).

In third-generation scanners the source-detector apparatus, or gantry, rotates around the patient. The source emits a continuous fan of x-rays which are partially absorbed, or attenuated, by bones and tissue. At discrete time intervals the intensities of the attenuated beams are recorded by a curved array detectors. These measurements are then used in a computerized algorithm to construct detailed images of the internal organs and structures of the body.

The quality of the image depends on both the detector density and the number of source locations. Since the x-ray source fires continuously throughout a scan, the source density can be increased without difficulty by increasing the number of measurements recorded by the detectors. The detector density, on the other hand, is fixed. Thus, the maximum image resolution is governed by the spacing of the detectors.

In third-generation scanners the detectors are placed side by side, without

any gaps, in order to catch the most x-rays. Unfortunately, this spacing limits the resolution to half of what the detectors are capable of measuring. If we wanted to use the standard algorithm (Algorithm 5.3 in [17]) to reconstruct at that higher resolution we would need to double both the source and the detector densities. While doubling the source density is not a problem, the detector density is fixed and the measured data would be undersampled by a factor of two. This predicament, which is inherent in the design of third-generation scanners, it is sometimes called the third-generation problem.

In this paper we discuss a new sampling scheme proposed by S. H. Izen, D. P. Rohler, and K.L.A. Sastry [4]. This method obtains the same resolution as the standard algorithm with just half the data. In practice, this allows for a doubling of the reconstruction resolution by doubling only the number of source locations, effectively solving the third-generation problem.

The paper is organized into six sections. In this section we cite the pertinent aspects of Fourier analysis and introduce the transforms used in two-dimensional tomography. Sampling theory is covered in Section 2, culminating with a periodic multi-dimensional sampling theorem developed by Faridani [5] [7]. The standard and the reflected sampling schemes are addressed in Section 3 including the benefits of the quarter detector shift. In Section 4 we discuss the method of Izen et al. for viewing the standard and reflected sample points as the union of shifted copies of a single rectangular lattice. Section 5 integrates Sections 2 and 4 and shows how the results can be applied to the third-generation problem, concluding with a numerical experiment verifying the results. A summary of our conclusions is found in Section 6

1.1 Fourier Analysis

We begin by introducing some notation that will be used in this paper. [14] [17] [10] [26].

Let $\mathbb{Z}, \mathbb{R}, \mathbb{C}$ denote the integers, real and complex numbers, respectively, and let χ_M be the characteristic function of a set M. $\mathbb{R}^n$ is the set of all real valued n-dimensional vectors, usually denoted by a single letter, $x = (x_1, x_2, \ldots, x_n), y = (y_1, y_2, \ldots, y_n)$, etc. The inner product on $\mathbb{R}^n$ is given by $\langle x, y\rangle = \sum_{i=1}^{n} x_i y_i$ and the absolute value of a vector is $|x| = \sqrt{\langle x, x\rangle}$. We denote the unit sphere in $\mathbb{R}^n$ by $S^{n-1} = \{x : |x| = 1\}$ and a point in S^{n-1} is usually designated by θ.

We say that a function f is in the space $C_0^\infty(\mathbb{R}^n)$ if f is infinitely differentiable and has compact support. $L^1(\mathbb{R}^n)$ is the space of (Lebesgue) integrable functions on $\mathbb{R}^n$ and $L^2(\mathbb{R}^n)$ is the space of square integrable functions. By $\mathcal{S}(\mathbb{R}^n)$ we denote the Schwartz space of rapidly decreasing functions. We note that $\mathcal{S}(\mathbb{R}^n)$ contains the space $C_0^\infty(\Omega)$ of infinitely differentiable functions which vanish outside of the unit disk Ω and that $\mathcal{S}(\mathbb{R}^n)$ is itself contained in $L^1(\mathbb{R}^n)$.

For $f \in L^1(\mathbb{R}^n)$ we define its Fourier transform $\hat{f}$ by

$$\hat{f}(\xi) = (2\pi)^{-n/2} \int_{\mathbb{R}^n} f(x) e^{-i\langle x,\xi\rangle} dx.$$

For large expressions we will consistently use $(\ldots)^\wedge$ for the Fourier transform of $(\ldots)$. The inverse Fourier transform $\tilde{f}$ of f is given by

$$\tilde{f}(\xi) = (2\pi)^{-n/2} \int_{\mathbb{R}^n} f(x) e^{i\langle x,\xi\rangle} dx.$$

Both transforms are used for other functions f such as those in $L^2(\mathbb{R}^n)$ and in $\mathcal{S}(\mathbb{R}^n)$ (see chapters 1 of [25] and 4 of [26]).

Fourier's inversion formula reads

$$\tilde{\hat{f}} = \hat{\tilde{f}} = f.$$

In fact, the Fourier transform maps $\mathcal{S}(\mathbb{R}^n)$ onto $\mathcal{S}(\mathbb{R}^n)$ linearly and continuously in both directions and $\tilde{f}$ is indeed the inverse mapping of $\hat{f}$ (see [26] pp. 146-147).

Some of the properties of the Fourier transform are as follows. Since it is linear we have

$$(af + bg)^\wedge = a\hat{f} + b\hat{g},$$

for any constants a and b. For $c > 0$ the scaling property

$$\hat{f}(c\,\xi) = c^{-n} \hat{f}\left(\frac{\xi}{c}\right),$$

holds. And if $y \in \mathbb{R}^n$, then the translation property of the Fourier transform is

$$\hat{f}(\xi + y) = e^{i\langle \xi, y\rangle} \hat{f}(\xi).$$

For f, g in $\mathcal{S}(\mathbb{R}^n)$ the convolution of f and g, written $f * g$, exists in $\mathcal{S}(\mathbb{R}^n)$ and is defined to be

$$\begin{aligned} f * g(x) &= \int_{\mathbb{R}^n} f(x-y) g(y) dy \\ &= \int_{\mathbb{R}^n} f(y) g(x-y) dy. \end{aligned}$$

It follows that the relations

$$\begin{aligned} (f * g)^\wedge &= (2\pi)^{n/2} \hat{f}\hat{g} \\ (fg)^\wedge &= (2\pi)^{-n/2} \hat{f} * \hat{g} \end{aligned}$$

also hold. Similar results exist for $\tilde{f}$.

We say that a function f is bandlimited with bandwidth b, or simply b-bandlimited, if $\hat{f}(\xi) = 0$ for $|\xi| \geq b$. In practice, the functions we deal with represent the densities of some tangible object. Such functions have compact support so their Fourier transforms do not vanish and they cannot be, strictly speaking, b-bandlimited. Consequently, we say f is *essentially* b-bandlimited if $\hat{f}(\xi)$ is suitably small for $|\xi| \geq b$ [14] [17]. The set $K = \mathrm{supp}(\hat{f}\,)$ is often called

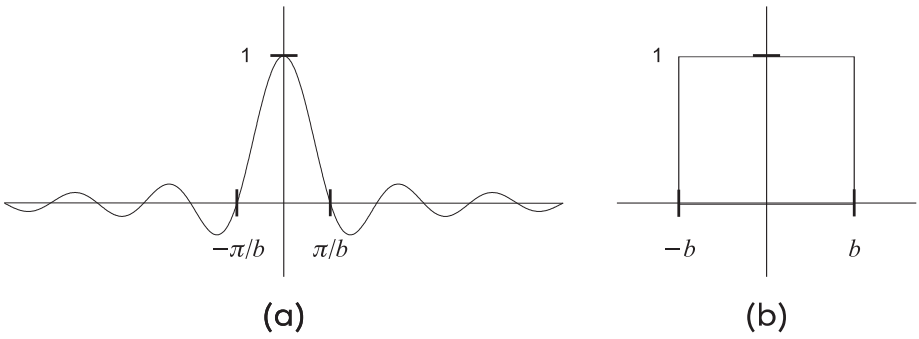

Figure 2: *Graph of (a)* $\mathrm{sinc}_b(x)$ *and (b)* $\chi_{[-b,b]}$

the bandregion of f. It is a generally accepted rule of thumb that b-bandlimited functions cannot represent details smaller than $2\pi/b$ [14] [17]. Accordingly, to see details of size d, the cut-off frequency b should be chosen large enough that $d \geq 2\pi/b$. Thus, higher bandwidths permit finer resolutions.

One very useful b-bandlimited function is $\mathrm{sinc}_b(x)$ where

$$\begin{aligned}
\mathrm{sinc}_b(x) &= \begin{cases} \frac{\sin bx}{bx} & \text{if } x \neq 0 \\ 1 & \text{if } x = 0 \end{cases} \\
&= \frac{1}{2ibx}(2i \sin bx) \\
&= \frac{1}{2ibx}\left(e^{ibx} - e^{-ibx}\right) \\
&= \frac{1}{2b}\int_{-b}^{b} e^{ix\xi} d\xi. \qquad (1.1)
\end{aligned}$$

The bandwidth of $\mathrm{sinc}_b(x)$ is b. To see this, consider the inverse Fourier transform of $\chi_{[-b,b]}$. We have

$$\begin{aligned}
\tilde{\chi}_{[-b,b]} &= (2\pi)^{-1/2}\int_{b}^{b} e^{ix\xi} dx \\
&= \frac{2b}{\sqrt{2\pi}}\,\mathrm{sinc}_b(\xi)
\end{aligned}$$

by (1.1). Then $\mathrm{sinc}_b(\xi) = \frac{\sqrt{2\pi}}{2b}\hat{\chi}_{[-b,b]}$ and by the Fourier inversion formula

$$\begin{aligned}
\widehat{\mathrm{sinc}_b}(\xi) &= \frac{\sqrt{2\pi}}{2b}\tilde{\hat{\chi}}_{[-b,b]} \\
&= \frac{\sqrt{2\pi}}{2b}\chi_{[-b,b]}.
\end{aligned}$$

Thus $\widehat{\text{sinc}_b}(\xi) = 0$ for $|\xi| \geq b$ or, in other words, $\text{sinc}_b(x)$ is b-bandlimited .

On the other hand, $\hat{\chi}_{-b,b} = \frac{2b}{\sqrt{2\pi}}\text{sinc}_b(\xi)$. But sinc_b is small outside of it's central lobe (i.e. outside $[-\pi/b,\ \pi/b]$). Thus, we can say that the essential bandwidth of $\chi_{-b,b}$ is π/b.

1.2 The Two-Dimensional Transforms

Here we introduce the standard transforms used in x-ray tomography. We will restrict ourselves to the two-dimensional case, though analogous results hold in R^n [14] [17].

In x-ray CT a beam of photons is sent through the patient. Some of the photons are absorbed or scattered and the intensity I of the beam after it has passed through the patient is measured. The function f which describes the absorption of the photons is called the x-ray attenuation coefficient. If we let L denote the ray along which the beam travels and I_0 the initial intensity of the beam, then the relation

$$I = I_0 e^{-\int_L f(x)dx}$$

or

$$\int_L f(x)dx = \log\left(\frac{I_0}{I}\right).$$

is known to hold [2]. Thus, measuring the intensity of the beam at a particular location provides us with the integral of f over some line L. The task is to reconstruct f given a finite number of its line integrals.

Usually the lines are arranged in a regular pattern, called a scanning geometry. Two common scanning geometries are the parallel beam and the fan beam (also called divergent beam [24]) geometries. The different geometries arise from different parameterizations of lines in $\mathbb{R}^2$ (see Figure 3).

Integrating f along the line $L(\varphi, s)$ perpendicular to $\theta = (\cos\varphi, \sin\varphi) \in S^1$ with signed distance s from the origin, produces the Radon transform

$$Rf(\varphi, s) = \int_{L(\varphi,s)} f(x)dx \tag{1.2}$$

$$= \int_{\mathbb{R}} f(s\theta + t\theta^{\perp})dt \tag{1.3}$$

where $\theta^{\perp} = (-\sin\varphi, \cos\varphi)$. It is common to write $Rf(\theta, s)$ for $Rf(\varphi, s)$ and to use $R_\varphi f(s)$ when φ is fixed. Since fixing φ produces a family of parallel lines, the Radon transform conveniently models parallel beam scanning.

The gantry of a parallel beam scanner consists of a single source and a single detector. During the scan a pencil thin beam of x-rays is translated across the patient while the detector moves in parallel on the opposite side. The gantry is then rotated and the process repeats.

Parallel beam geometry was used in first-generation CT scanners. Reliance on a single detector meant that a single scan often took several minutes, an uncomfortably long time for patients. Manufacturers of medical CT scanners have

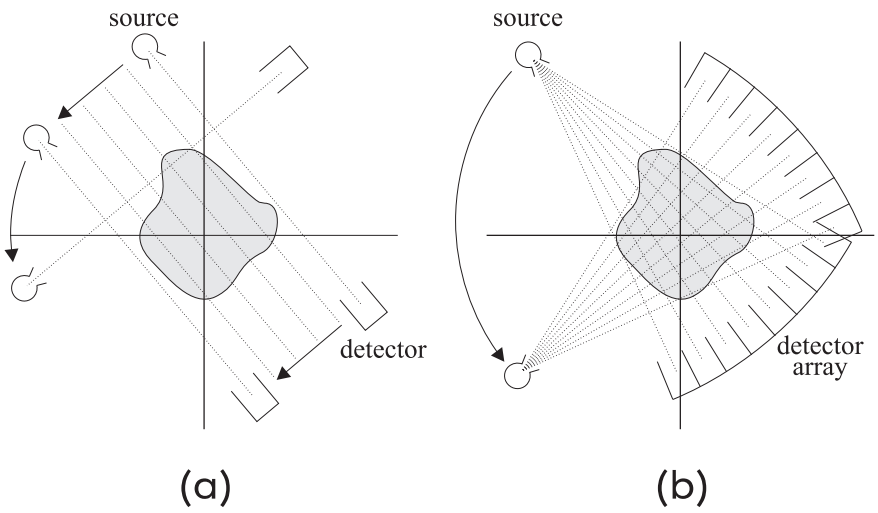

Figure 3: *Scanning geometries in 2D tomography: (a) parallel beam, used in first-generation scanners (b) fan beam, used in current third-generation scanners.*

replaced parallel beam scanning with faster methods that are able to measure hundreds of rays simultaneously.

The gantry of a third-generation scanner contains of a single x-ray source and a curved array of about 500-1000 detectors. The source is switched on and the gantry rotates around the patient. At discrete time intervals during the rotation the detectors record the intensities of the x-rays. It is sometimes helpful to visualize the equivalent scenario of a single source firing out a fan of individual beams at a number of precise locations throughout the rotation. This technique is extremely fast and efficient. Often hundreds of thousands of measurements are captured in a single 2π rotation which typically takes less than 2 seconds.

To model fan beam scanning let r be the radius of the source circle and let $a = r(\cos\alpha, \sin\alpha)$ be a point on that circle. We always assume that $r > \rho > 0$, where ρ is the radius of the circle which contains the object being imaged (scan circle). The point a is the source of the ray $L(\alpha, \beta)$ which makes the angle β with the line (central ray) joining a to the origin (see Figure 4). By convention, β is positive if, when viewed from the source point a, the ray $L(\alpha, \beta)$ is left of the central ray. We limit β to the interval $[-\pi/2, \pi/2]$ and in practice $-\arcsin(\rho/r) \leq \beta \leq \arcsin(\rho/r)$. Now an entire fan of beams can be described by simply varying the parameter β.

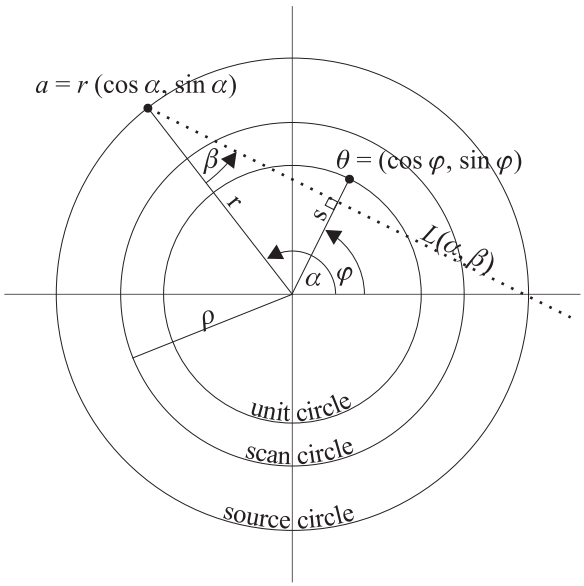

Figure 4: *Parameters φ, s of the 2D Radon transform and α, β of the fan beam transform. The angles φ and α are measured counterclockwise from the x-axis, and β is measured counterclockwise from the line connecting the point a to the origin.*

Integrating f along $L(\alpha, \beta)$ gives the fan beam (or divergent beam) transform

$$Df(\alpha, \beta) = \int_{L(\alpha,\beta)} f(x)dx.$$

The parallel beam and fan beam parameterizations are related by

$$s = r \sin \beta, \qquad \varphi = \alpha + \beta - \pi/2$$

(see Figure 4). Thus,

$$Df(\alpha, \beta) = Rf(\alpha + \beta - \pi/2, r \sin \beta). \tag{1.4}$$

Both Rf and Df have a symmetry property, which reads

$$Rf(\varphi, s) = Rf(\varphi + \pi, -s)$$

for the Radon transform and

$$Df(\alpha, \beta) = Df(\pi + \alpha + 2\beta, -\beta) \tag{1.5}$$

for the fan beam transform. These are easily verified by inspection. This means that every measurement can be used twice, once at the actual sample point

and again at the reflected point. In Section 3.3 we will discuss how to use the reflected data in the fan beam geometry.

Lastly, the Fourier transform of $R_\varphi f$ is

$$\begin{aligned}\widehat{R_\varphi f}(\sigma) &= (2\pi)^{-1/2} \int_{\mathbb{R}} R_\varphi f(s) e^{-is\sigma} ds \\ &= (2\pi)^{1/2} \hat{f}(\sigma\theta). \end{aligned} \tag{1.6}$$

This is called the projection-slice or Fourier-slice theorem [14] [10]. It is a key element of several reconstruction algorithms including the well-known filtered back projection.

2 Sampling Theory

In practice we can only collect a finite set of measurements. Questions concerning how to choose those measurements are addressed by sampling theorems. Sampling theorems give conditions under which a function can be recovered from its values on a discrete set. We begin with Shannon's sampling theorem and build to a more general multi-dimensional sampling theorem by Faridani that is central to this paper.

2.1 Shannon's Sampling Theorem

Shannon's classical sampling theorem [21] applies to b-bandlimited functions on $\mathbb{R}$. It reads:

Theorem 1. *Let f be a b-bandlimited function on $L^2(\mathbb{R})$ and let*

$$0 < h \leq \pi/b. \tag{2.1}$$

Then

$$f(x) = \sum_{k\in\mathbb{Z}} f(kh)\,\mathrm{sinc}_b(x - kh).$$

Thus, f is completely determined by its values on an set of equally spaced points on the real line provided the spacing is no larger than π/b. Condition (2.1) is often called the Nyquist condition.

2.2 Multi-Dimensional Sampling Theorems

In multiple dimensions the sampling sets become lattices, i.e. the images of $\mathbb{Z}^n$ under some linear transformation.

If W is a real non-singular (n, n) matrix then such a lattice can be described as

$$L_W = \{Wk : k \in \mathbb{Z}^n\} = W\mathbb{Z}^n, \tag{2.2}$$

and we say that L_W is the lattice generated by W. The reciprocal lattice, or dual lattice, $L_W^\perp$ is defined to be the lattice generated by the matrix $2\pi(W^{-1})^T$.

We remark that while L_W does not uniquely determine the generator matrix W, it does determine the determinant of W and the dual lattice.

Just as points on the real line needed to satisfy the Nyquist condition, a lattice must satisfy a density requirement in order to be suitable for sampling a given function f. As we will see in Theorem 2, this density requirement depends on the size and shape of the set $K = \text{supp}(\hat{f}\,)$.

We are now able to state the Petersen-Middleton sampling theorem, which extends Shannon's results to $\mathbb{R}^n$ (reference pp 289 of [20] and Theorem 2.1 of [5]).

Theorem 2. *Let K be a compact subset of $\mathbb{R}^n$, W a real non-singular (n,n) matrix such that*

$$\text{the translates } \; K+\eta,\, \eta \in L_W^{\perp} \; \text{ are disjoint.} \tag{2.3}$$

If $f \in \mathcal{S}(\mathbb{R}^n)$ with $\hat{f} = 0$ outside of K, then

$$f(x) = \sum_{k\in\mathbb{Z}^n} f(Wk)g(x-Wk) \tag{2.4}$$

where $g(y) = (2\pi)^{(-n/2)}|\det W|\hat{\chi}_K(-y)$.

The requirement (2.3) that translates of K by elements of $L_W^{\perp}$ be disjoint is a generalization of the Nyquist condition (2.1) to lattices. Since the densities of L_W and $L_W^{\perp}$ are inversely proportional, when (2.3) is satisfied L_W is a sufficiently dense sampling set.

We now work toward a generalization of Theorem 2.

Suppose that L_W is too sparse to satisfy the sampling condition (2.3). Then the set K is overlapped by one or more of the translates $K+\eta, \eta \in L_W^{\perp}$. We can partition K by grouping together the regions which are covered by the same translates.

As a simple example, consider Figure 5. Here the translates

$$\begin{aligned} &K - 2\pi \left(W^{-1}\right)^T (0,-1)^T && \text{(dashed)},\\ &K - 2\pi \left(W^{-1}\right)^T (0,1)^T && \text{(dotted)}, \end{aligned}$$

intersect the set

$$K = K - 2\pi \left(W^{-1}\right)^T (0,0)^T \qquad \text{(solid)},$$

and divide it into three distinct regions. The first region, K_1, is the portion of K which is covered only by the identity translate $K = K - 2\pi \left(W^{-1}\right)^T (0,0)^T$. The second area, K_2, is the region where K is overlapped by both $K - 2\pi \left(W^{-1}\right)^T (0,-1)^T$ and the identity translate. Both the identity and $K - 2\pi \left(W^{-1}\right)^T (0,1)^T$ cover K_3. It follows that the decomposition of K is $K = K_1 \cup K_2 \cup K_3$.

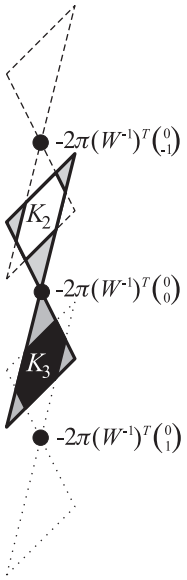

Figure 5: *Decomposition of the set K into mutually disjoint subsets K_1 (union of the gray sections), K_2 (white), and K_3 (black) by the translates $K-2\pi\left(W^{-1}\right)^T(0,0)^T$, $K-2\pi\left(W^{-1}\right)^T(0,-1)^T$, and $K-2\pi\left(W^{-1}\right)^T(0,1)^T$, respectively.*

To make the decomposition of K more precise, for $\xi \in K$,let

$$\begin{aligned} M_\xi &= \left\{ k \in \mathbb{Z}^n : \xi - 2\pi \left(W^{-1}\right)^T k \in K \right\} \\ &:= \left\{ k_{\xi 1},\, \ldots,\, k_{\xi m_\xi} \right\}. \end{aligned}$$

As each region of the decomposition is covered by the identity translate we can let $k_{\xi 1} = 0$ with out loss of generality. The M_ξ will only assume finitely many different values $M_1, \ldots, M_L$. In the above example we have

$$\begin{aligned} M_1 &= \{k_{11} = (0,0)^T\} \\ M_2 &= \{k_{21} = (0,0)^T,\ k_{22} = (0,-1)^T\} \\ M_3 &= \{k_{31} = (0,0)^T,\ k_{32} = (0,1)^T\}. \end{aligned}$$

We can now define each K_l to be the disjoint sets

$$K_l = \{\xi \in K : M_\xi = M_l\}, \tag{2.5}$$

and formally decompose K by $K = \bigcup_{l=1}^{L} K_l$.

In higher dimensions, or when the number of overlaps is large, decomposing K can be a daunting task and algorithms like those developed [7] should be

used. For our purposes in this paper, much can be done by simply drawing the translated sets.

We are now able to generalize the Petersen-Middleton theorem. Instead of using L_W, we take as our sampling set the union of m of shifted copies of L_W. That is, lattices of the form $L_W + a_r, a_r \in \mathbb{R}^n, r = 1, \ldots, m$. The number m turns out to be the maximum number of overlappings of the K_l. The following theorem is due to Faridani (see Theorem 2.2 in [5]).

Theorem 3. *Let $K_l \subset \mathbb{R}^n, l = 1, \ldots, L$ be mutually disjoint bounded measurable sets, $K = \bigcup_{l=1}^{L} K_l$, and W a real non-singular (n, n) matrix such that (2.5) holds. Further, let $m = max_{1 \le l \le L}(m_l)$ and $a_1, \ldots, a_m \in \mathbb{R}^n$ such that there exist coefficients $b_r^l \in \mathbb{C}, r = 1, \ldots, m; l = 1, \ldots, L$ satisfying the equations*

$$\sum_{r=1}^{m} b_r^l = 1 \tag{2.6}$$

$$\sum_{r=1}^{m} b_r^l e^{-2\pi i \langle W^{-1} a_r,\, k_{lj} \rangle} = 0, \quad j = 2, \ldots, m_l \tag{2.7}$$

for $l = 1, \ldots, L$. If $f \in \mathcal{S}(\mathbb{R}^n)$ and $\hat{f} = 0$ outside of K, then

$$f(x) = \sum_{r=1}^{m} \sum_{k \in \mathbb{Z}^n} f(a_r + Wk) g_r(x - a_r - Wk) \tag{2.8}$$

where

$$g_r(y) = (2\pi)^{-n/2} |\det W| \sum_{l=1}^{L} b_r^l \hat{\chi}_{K_l}(-y). \tag{2.9}$$

The idea of the proof is to compute the Fourier transform of the right-hand side of (2.8) and show that it is $\hat{f}$. This is done using Poisson's summation formula which, in this setting, reads

$$(2\pi)^{-n/2} |\det W| \sum_{k \in \mathbb{Z}^n} f(Wk) e^{-i\langle \xi,\, Wk \rangle} = \sum_{k \in \mathbb{Z}^n} \hat{f}(\xi - 2\pi (W^{-1})^T k).$$

As the techniques are similar to those used in Theorem 4, we omit the details of the proof. Note that Theorem 2 is obtained from Theorem 3 in the case of $m = L = 1$.

2.3 A Periodic Multi-Dimensional Sampling Theorem

To this point we have only considered sampling theory on $\mathbb{R}^n$. Often the functions of interest in tomography are periodic in some of their variables. For example, Rf is periodic in its first variable and Df is periodic in both. We need an extension of Theorem 3 to the periodic setting.

Functions which are periodic in some of their variables can be regarded as being defined on the group $T^{n_1} \times \mathbb{R}^{n_2} \subset \mathbb{R}^n$, $n = n_1 + n_2$ where $T = \mathbb{R}/2\pi\mathbb{Z}$ is

the circle (torus) group. We take the interval $[0, 2\pi)$ with addition modulo 2π as a model for T and the Lebesgue measure $d\varphi$ on T is the restriction of the Lebesgue measure on $\mathbb{R}$ to $[0, 2\pi)$.

For $f : \mathbb{R}^{n_1} \times \mathbb{R}^{n_2} \to \mathbb{C}$ define $f_y(\varphi) : \mathbb{R}^{n_1} \to \mathbb{C}$ and $f_\varphi(y) : \mathbb{R}^{n_2} \to \mathbb{C}$ by $f_y(\varphi) = f(y, \varphi) = f_\varphi(y)$ Let S^{n_1,n_2} denote the set of infinitely continuously differentiable functions which are 2π-periodic in their first n_1 variables. That is,

$$\begin{aligned} S^{n_1,n_2} = \{f \in C^\infty(\mathbb{R}^{n_1} \times \mathbb{R}^{n_2}) : \forall y \in \mathbb{R}^{n_2},\ f_y(\varphi) \text{ is } 2\pi\text{-periodic and} \\ \forall \varphi \in \mathbb{R}^{n_1},\ f_\varphi(y) \in L^2(\mathbb{R}^{n_2})\}. \end{aligned}$$

Let $f \in S^{n_1,n_2}$. The Fourier transform $\hat{f}$ on $T^{n_1} \times \mathbb{R}^{n_2}$ is defined to be

$$\begin{aligned} \hat{f} &: \mathbb{Z}^{n_1} \times \mathbb{R}^{n_2} \to \mathbb{C} \\ \hat{f}(\xi) &= (2\pi)^{-(n_1+n_2)/2} \int_{T^{n_1} \times \mathbb{R}^{n_2}} f(x) e^{-i\langle x,\xi\rangle} dx \\ &= (2\pi)^{-(n_1+n_2)/2} \int_{T^{n_1}} \int_{\mathbb{R}^{n_2}} f(\varphi, y) e^{-i\langle \varphi,\nu\rangle - i\langle y,\sigma\rangle} dy d\varphi \end{aligned}$$

with $x = (\varphi, y) \in T^{n_1} \times \mathbb{R}^{n_2}$, $\xi = (\nu, \sigma) \in \mathbb{Z}^{n_1} \times \mathbb{R}^{n_2}$. The inverse Fourier transform is given by

$$\tilde{g}(x) = (2\pi)^{(n_1+n_2)/2} \int_{\mathbb{Z}^{n_1} \times \mathbb{R}^{n_2}} g(\xi) e^{i\langle x,\xi\rangle} d\xi$$

where $d\xi$ denotes the product of the discrete measure on $\mathbb{Z}^{n_1}$ and the Lebesgue measure on $\mathbb{R}^{n_2}$, i.e.

$$\tilde{g}(x) = (2\pi)^{(n_1+n_2)/2} \sum_{\nu \in \mathbb{Z}^{n_1}} \int_{\mathbb{R}^{n_2}} g(\xi) e^{i\langle \varphi,\nu\rangle + i\langle y,\sigma\rangle} d\sigma.$$

If f is defined on $T^{n_1} \times \mathbb{R}^{n_2}$ then sampling on a generic lattice L_W as defined in (2.2) may not yield accurate results. In order to correctly sample a periodic function a lattice must have the same periods as f, that is, it must be a discrete subgroup of $T^{n_1} \times \mathbb{R}^{n_2}$. Such lattices are called *sampling lattices*. To make this more precise we need the following definition (reference Definition 5.1 in [12]):

Definition 1. *A real nonsingular (n_1+n_2, n_1+n_2) matrix W is called* feasible *if $2\pi e_i \in W\mathbb{Z}^{n_1+n_2}$ for $i = 1, \ldots, n_1$ where the e_i denote the canonical unit vectors of $\mathbb{R}^{n_1+n_2}$.*

A feasible $(n_1 + n_2, n_1 + n_2)$ matrix W generates a lattice in $\mathbb{R}^{n_1+n_2}$ which is 2π periodic in its first n_1 components. That is, for $x \in \mathbb{R}^{n_1}$, $y \in \mathbb{R}^{n_2}$,

$$\begin{pmatrix} x \\ y \end{pmatrix} \in \{Wk : k \in \mathbb{Z}^{n_1+n_2}\} \iff \begin{pmatrix} x + 2\pi j \\ y \end{pmatrix} \in \{Wk : k \in \mathbb{Z}^{n_1+n_2}\}$$

for all $j \in \mathbb{Z}^{n_1}$. For a feasible matrix W, if let $A_W = \{k \in \mathbb{Z}^{n_1+n_2} : Wk \in [0, 2\pi)^{n_1} \times \mathbb{R}^{n_2}\}$, then the set $\{Wk : k \in A_W\}$ is a discrete subgroup of $T^{n_1} \times \mathbb{R}^{n_2}$. Formally, we have

Definition 2. *For a feasible* $(n_1+n_2,\ n_1+n_2)$ *matrix* W*, the set*

$$L_W = \{Wk : k \in A_W\}, \quad A_W = \{k \in \mathbb{Z}^{n_1+n_2} : Wk \in [0,2\pi)^{n_1} \times \mathbb{R}^{n_2}\}$$

is called the sampling lattice *generated by* W*. The set*

$$L_W^{\perp} = 2\pi \left(W^{-1}\right)^T \mathbb{Z}^{n_1+n_2}$$

is called the dual lattice *with respect to* L_W*.*

For practical reasons, we would like more than one measurement to be taken for each occurring source angle. Sampling lattices which satisfy this additional condition are called *admissible sampling lattices* [6] [9].

We now state the main theorem of this section, which is due to Faridani (see Theorem 2.3 in [5]).

Theorem 4. *Let* $K_l \subset \mathbb{Z} \times \mathbb{R}$, $l = 1, \ldots, L$ *be mutually disjoint bounded measurable sets,* $K = \bigcup_{l=1}^{L} K_l$*, and* W *a feasible* (n_1+n_2, n_1+n_2) *matrix such that (2.5) holds for* $n = n_1 + n_2$*.*

Further, let $m = \max_{1\le l\le L}(m_l)$ *and* $a_1, \ldots, a_m \in \mathbb{R}^2$ *be such that there exist coefficients* $b_r^l \in \mathbb{C}$, $r = 1, \ldots, m$; $l = 1, \ldots, L$ *satisfying the equations (2.6) and (2.7) for* $l = 1, \ldots, L$*.*

For $f \in S^{n_1,n_2}$ *define*

$$S_W f(x) = \sum_{r=1}^{m} \sum_{k\in A_W} f(a_r + Wk) g_r(x - a_r - Wk) \tag{2.10}$$

with

$$g_r(y) = (2\pi)^{-(n_1+n_2)/2} |\det W| \sum_{l=1}^{L} b_r^l \, \widetilde{\chi}_{K_l}(y).$$

Under these conditions the following error estimate holds:

$$|S_W f(x) - f(x)| \le (2\pi)^{-(n_1+n_2)/2}(1+\gamma) \int_{(\mathbb{Z}^{n_1}\times\mathbb{R}^{n_2})\setminus K} |\hat{f}(\xi)| d\xi$$

where

$$\gamma = m \left(\max_{1\le l\le L} \sum_{r=1}^{m} |b_r^l| \right). \tag{2.11}$$

Proof. Let $n = n_1 + n_2$. The Poisson summation formula for $L_W = \{Wk : k \in A_W\} \subset T^{n_1} \times \mathbb{R}^{n_2}$ reads

$$(2\pi)^{-n/2} |\det W| \sum_{k\in A_W} f(Wk) = \sum_{k\in\mathbb{Z}^n} \hat{f}(2\pi \left(W^{-1}\right)^T k),$$

see, for example, Lemma 5.2 in [12]. With this we find that

$$\begin{aligned} &(2\pi)^{-n/2} |\det W| \sum_{k\in A_W} f(a_r + Wk) e^{-i\langle \xi, Wk\rangle} \\ &= \sum_{k\in\mathbb{Z}^n} \hat{f}(\xi - 2\pi \left(W^{-1}\right)^T k) e^{-2\pi i \langle W^{-1}a_r, k\rangle} e^{i\langle a_r, \xi\rangle}. \end{aligned} \tag{2.12}$$

Using this relation and the fact that $\chi_{K_l} = \widehat{\widetilde{\chi}}_{K_l}$ we obtain

$$
\begin{aligned}
&(S_W f)^\wedge = \\
&\left[\sum_{r=1}^{m} \sum_{k \in A_W} f(a_r + Wk) g_r(\,\cdot\, - a_r - Wk)\right]^\wedge (\xi) \\
&= \left[\sum_{r=1}^{m} \sum_{k \in A_W} f(a_r + Wk)(2\pi)^{-n/2} |\det W| \sum_{l=1}^{L} b_r^l \widetilde{\chi}_{K_l}(\,\cdot\, - a_r - Wk)\right]^\wedge (\xi) \\
&= \left[\sum_{r=1}^{m} \sum_{k \in A_W} f(a_r + Wk)(2\pi)^{-n/2} |\det W| \sum_{l=1}^{L} b_r^l \widetilde{\chi}(\,\cdot\,) e^{-i\langle\,\cdot\,,\, a_r + Wk\rangle}\right]^\wedge (\xi) \\
&= \sum_{r=1}^{m} \sum_{k \in A_W} f(a_r + Wk)(2\pi)^{-n/2} |\det W| \sum_{l=1}^{L} b_r^l \chi_{K_l}(\xi) e^{-i\langle \xi,\, a_r + Wk\rangle} \\
&= \sum_{r=1}^{m} \left((2\pi)^{-n/2} |\det W| \sum_{k \in A_W} f(a_r + Wk) e^{-i\langle \xi,\, Wk\rangle}\right) \sum_{l=1}^{L} b_r^l \chi_{K_l}(\xi) e^{-i\langle \xi,\, a_r\rangle} \\
&= \sum_{r=1}^{m} \sum_{k \in \mathbb{Z}^n} \hat{f}\left(\xi - 2\pi \left(W^{-1}\right)^T k\right) e^{-2\pi i \langle W^{-1} a_r,\, k\rangle} e^{-i\langle a_r,\, \xi\rangle} \sum_{l=1}^{L} b_r^l \chi_{K_l}(\xi) e^{-i\langle \xi,\, a_r\rangle} \\
&= \sum_{l=1}^{L} \chi_{K_l}(\xi) \sum_{k \in \mathbb{Z}^n} \hat{f}\left(\xi - 2\pi \left(W^{-1}\right)^T k\right) \sum_{r=1}^{m} b_r^l e^{-2\pi i \langle W^{-1} a_r,\, k\rangle}.
\end{aligned}
$$

Now we split the sum over k into two parts, one with $k \in M_l$ and the other with $k \in \mathbb{Z}^n \backslash M_l$. If k only runs through M_l and using equations (2.6, 2.7) we have

$$
\begin{aligned}
&\sum_{l=1}^{L} \chi_{K_l}(\xi) \sum_{j=1}^{m_l} \hat{f}\left(\xi - 2\pi \left(W^{-1}\right)^T k_{l\,j}\right) \sum_{r=1}^{m} b_r^l e^{-2\pi i \langle W^{-1} a_r,\, k_{l\,j}\rangle} \\
&= \sum_{l=1}^{L} \chi_{K_l}(\xi) \hat{f}(\xi) \\
&= \chi_K(\xi) \hat{f}(\xi).
\end{aligned}
$$

This leads to

$$
\begin{aligned}
&|S_W f(x) - f(x)| \\
&\leq (2\pi)^{-n/2} \int_{\mathbb{Z}^{n_1}\times\mathbb{R}^{n_2}} |(S_W f)^\wedge(\xi) - \hat{f}(\xi)| d\xi \\
&\leq (2\pi)^{-n/2} \int_{\mathbb{Z}^{n_1}\times\mathbb{R}^{n_2}} (1 - \chi_K(\xi))|\hat{f}| d\xi \\
&+ (2\pi)^{-n/2} \int_{\mathbb{Z}^{n_1}\times\mathbb{R}^{n_2}} \left| \sum_{l=1}^{L} \chi_{K_l}(\xi) \sum_{k\in\mathbb{Z}^n\setminus M_l} \hat{f}(\xi - 2\pi \left(W^{-1}\right) k) \sum_{r=1}^{m} b_r^l e^{-2\pi i \langle W^{-1} a_r\, ,\, k\rangle} \right| d\xi \\
&= (2\pi)^{-n/2} \int_{(\mathbb{Z}^{n_1}\times\mathbb{R}^{n_2})\setminus K} |\hat{f}(\xi)| d\xi \\
&+ (2\pi)^{-n/2} \sum_{l=1}^{L}\sum_{r=1}^{m} |b_r^l| \sum_{k\in\mathbb{Z}^n\setminus M_l} \int_{K_l - 2\pi(W^{-1})^T k} |\hat{f}(\xi)| d\xi. \qquad (2.13)
\end{aligned}
$$

The assumption (2.5) implies that $(K_l - 2\pi \left(W^{-1}\right)^T k) \cap K = \emptyset$ if $k \in \mathbb{Z}^n \setminus M_l$. Further, for each $\xi \in (\mathbb{Z}^{n_1}\times\mathbb{R}^{n_2})\setminus K$ there exist no more than m different $k \in \mathbb{Z}^n$ such that $\xi \in K - 2\pi \left(W^{-1}\right)^T k$. Using this and the fact that the K_l are mutually disjoint, we have for the last term of the inequality above

$$
\begin{aligned}
&\sum_{l=1}^{L}\sum_{r=1}^{m} |b_r^l| \sum_{k\in\mathbb{Z}^n\setminus M_l} \int_{K_l - 2\pi(W^{-1})^T k} |\hat{f}(\xi)| d\xi \\
&\leq \left(\max_{1\leq l\leq L} \sum_{r=1}^{m} |b_r^l| \right) \sum_{k\in\mathbb{Z}^n} \sum_{l=1}^{L} \int_{(K_l - 2\pi(W^{-1})^T k)\setminus K} |\hat{f}(\xi)| d\xi \\
&= \left(\max_{1\leq l\leq L} \sum_{r=1}^{m} |b_r^l| \right) \sum_{k\in\mathbb{Z}^n} \int_{(K - 2\pi(W^{-1})^T k)\setminus K} |\hat{f}(\xi)| d\xi \\
&\leq m \left(\max_{1\leq l\leq L} \sum_{r=1}^{m} |b_r^l| \right) \int_{(\mathbb{Z}^{n_1}\times\mathbb{R}^{n_2})\setminus K} |\hat{f}(\xi)| d\xi.
\end{aligned}
$$

Inserting this into (2.13) yields the desired estimate. □

We note that if $\mathrm{supp}(\hat{f}\,) = K$, then $(S_W f)^\wedge = \hat{f}$ and f would be given by (2.10). If f is essentially b-bandlimited, then the right hand side of (5.8) is small [18] and (2.10) can still be used to compute f. We will use this fact later on. If, in addition, $n_1 = 0$, then we obtain Theorem 3.

3 Sampling Geometry

In this section we determine the shape of the set K and appropriate lattices L_W so that the results of Section 2 hold for Df. We also discuss how to use the reflection property (1.5) of Df to increase the number of data points.

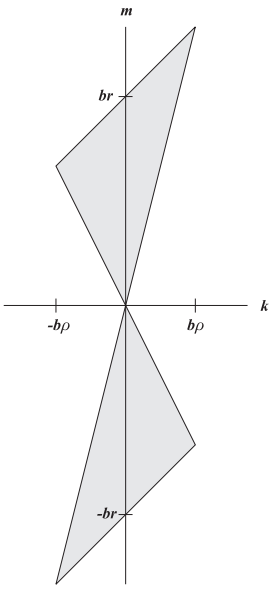

Figure 6: *Essential support* K *of* $\widehat{Df}$ *when* $\rho/r = 1/3$.

3.1 Support of $\widehat{Df}$

The fan beam transform is periodic in both arguments and can be viewed as a function on the group $T \times T = T^2$. The Fourier transform of Df is

$$\widehat{Df}(s,t) = \frac{1}{4\pi^2} \int_0^{2\pi} \int_0^{2\pi} Df(\alpha,\beta) e^{-is\alpha - it\beta} d\beta d\alpha, \quad s,t \in \mathbb{Z}, \tag{3.1}$$

(reference pg. 75 of [17]). It has been shown [15] [18] that $\widehat{Df}$ is small outside the set

$$K = \{(s,t) \in \mathbb{Z}^2 : |s-t| < br, |s|r < |s-t|\rho\} \tag{3.2}$$

where b is the bandwidth of f, $\rho > 0$ is the scan radius, and $r > \rho$ is the source radius. Thus, K is the essential support of f. This is the region bounded by the lines

$$\begin{aligned} t &= s + br, & t &= s - br, \\ s &= t + \frac{s\,r}{\rho}, & t &= s - \frac{s\,r}{\rho}, \end{aligned}$$

as seen in Figure 6. The set K will help us select appropriate sampling lattices.

3.2 Sampling Schemes

In Section 2 it was shown that accurate reconstruction requires the lattice L_W to be sufficiently dense. However, to avoid excessive computation, we would

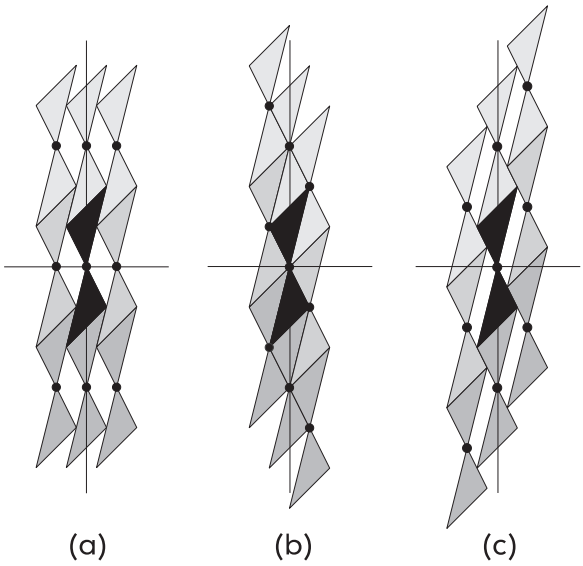

Figure 7: *Translates of K with respect to the dual lattice $L_W^\perp$ for (a) the standard lattice, (b) the efficient lattice, and (c) the reflected samples for fan beam scanning. Dots indicate elements of $L_W^\perp$. K is in black.*

like L_W to be as sparse as possible. Thus, we seek lattices L_W for which the translated sets $K + \eta$, $\eta \in L_W^\perp$ are disjoint, but as densely packed as possible.

Under the standard sampling scheme the sampled points are (α_j, β_l) where

$$\alpha_j = j\Delta\alpha, \qquad \beta_l = l\Delta\beta, \qquad j, l \in \mathbb{Z} \tag{3.3}$$

$$\Delta\alpha = \frac{2\pi}{p}, \qquad \Delta\beta = \frac{\pi}{q}, \qquad p, q \in \mathbb{Z}. \tag{3.4}$$

The sampling lattice L_W and its dual lattice $L_W^\perp$ are generated by

$$W = \begin{pmatrix} \Delta\alpha & 0 \\ 0 & \Delta\beta \end{pmatrix}, \qquad W^\perp = \begin{pmatrix} 2\pi/\Delta\alpha & 0 \\ 0 & 2\pi/\Delta\beta \end{pmatrix}, \tag{3.5}$$

and the sets $K + \eta, \eta \in L_W^\perp$ are simply vertical and horizontal translates of K (see Figure 7a). These translates are disjoint if and only if

$$\Delta\alpha \leq \frac{r+\rho}{\rho}\frac{\pi}{br}, \qquad \Delta\beta \leq \frac{\pi}{br}. \tag{3.6}$$

Violating these sampling conditions (3.6) may cause artifacts in the reconstructed image (see [17] pg. 76).

In the standard scheme the translates do not completely fill $\mathbb{R}^2$, so it is not

efficient. However, if

$$W = \begin{pmatrix} \Delta\alpha & \frac{r-\rho}{2r}\Delta\alpha \\ 0 & \Delta\beta \end{pmatrix}, \qquad W^{\perp} = \begin{pmatrix} 2\pi/\Delta\alpha & 0 \\ \frac{\pi(r-\rho)}{r\Delta\beta} & 2\pi/\Delta\beta \end{pmatrix},$$

with

$$\Delta\alpha = \frac{2\pi}{b\rho}, \qquad \Delta\beta = \frac{\pi}{br}.$$

then the plane is completely covered (see Figure 7b). This efficient scheme was introduced by Natterer in [15] and achieves the same reconstruction quality as the standard geometry but with significantly less data. The efficient geometry requires the detector array to be shifted every time the source moves from one position to the next. Natterer has stated that it is difficult to implement this efficient scanning geometry for a commercial scanner (see pg. 77 in [17]).

A third sampling geometry is possible if we use only the reflections of the sample points. Recalling the symmetry property of the fan beam transform

$$Df(\alpha, \beta) = Df(\pi + \alpha + 2\beta, -\beta), \tag{3.7}$$

we see that if the original sample points are given by (3.3), then the reflected points $(\alpha'_{j,l}, \beta'_l)$ are

$$\alpha'_{j,l} = \pi + j\Delta\alpha + 2l\Delta\beta, \qquad \beta'_l = -l\Delta\beta. \tag{3.8}$$

This corresponds to choosing

$$W = \begin{pmatrix} \Delta\alpha & 2\Delta\beta \\ 0 & -\Delta\beta \end{pmatrix}, \qquad W^{\perp} = \begin{pmatrix} 2\pi/\Delta\alpha & 0 \\ 4\pi/\Delta\alpha & -2\pi/\Delta\beta \end{pmatrix}. \tag{3.9}$$

As with the standard geometry, the translates $K + \eta, \eta \in L^{\perp}_W$ are disjoint if and only if (3.6) holds (see Figure 7c).

Since the reflected samples are always available, one could logically ask if it would be possible to double the number of data points by using both the standard and the reflected points. It is possible, but first we must eliminate any redundancy in the scanning geometry, that is, we must avoid having the reflected sample points and the standard sampling points represent the same lines. This is done with a shift in the detector array.

3.3 The Quarter Detector Shift

When the detector array is centered, the central ray of the fan intersects the center of the detector on the opposite side (see Figure 8a). During a scan some measurements may, as in Figure 8b, duplicate each other. However, shifting the detector array slightly off center by a fixed amount $\delta\Delta\beta,\ 0 \leq \delta < 1$, can break that symmetry (see Figure 8d).

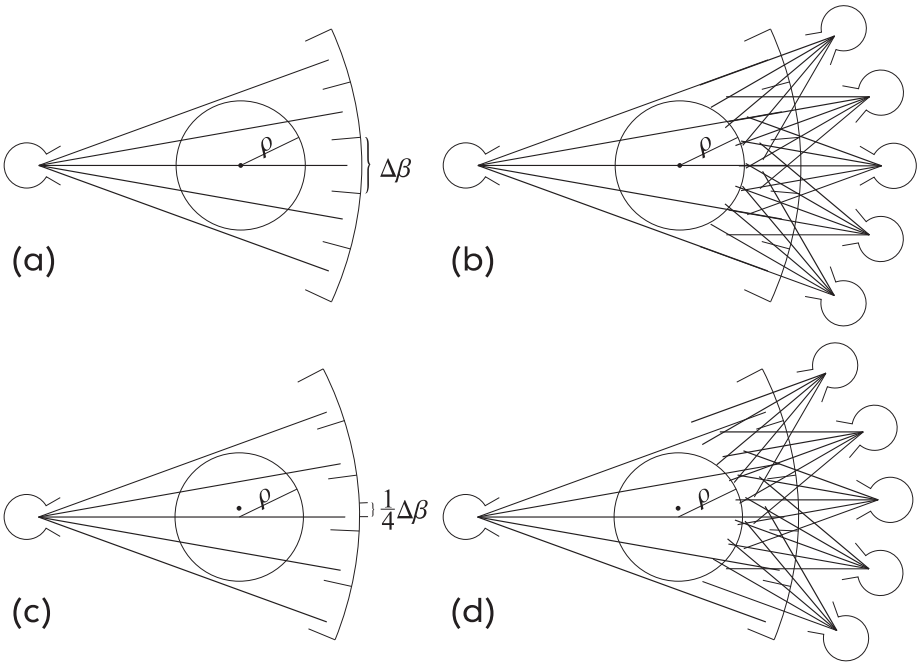

Figure 8: *When the detector array is centered (a) the offset is 0 and some views may duplicate one another (b). If the array is offset by $\delta = 1/4$ of the width of a detector (c) then there is no redundancy (d). Dots indicate the center of gantry's rotation which, when $\delta = 1/4$, is different from the center of the scan circle. Example shown for $\Delta\alpha = 2\pi/9$, $\Delta\beta = \pi/9$.*

When a detector shift is used with the standard scheme we obtain the original lattice $L_O = \{(\alpha_j, \beta_l)\}$ where

$$\alpha_j = j\Delta\alpha, \qquad \beta_l = (l+\delta)\Delta\beta, \qquad j, l \in \mathbb{Z} \tag{3.10}$$

$$\Delta\alpha = \frac{2\pi}{p}, \qquad \Delta\beta = \frac{\pi}{q}, \qquad p, q \in \mathbb{Z}. \tag{3.11}$$

In reality we only need $j = 0, \ldots, p-1$ and $l = -Q, \ldots, Q$ with $Q \geq \frac{\arcsin(\rho/r)}{\Delta\beta}$ since Df is either 0 or can be computed by periodicity otherwise.

The corresponding reflected samples $L_R = \{(\alpha'_{j,l}, \beta'_l)\}$ are given by

$$\alpha'_{j,l} = \pi + j\Delta\alpha + 2(l+\delta)\Delta\beta, \qquad \beta'_l = -(l+\delta)\Delta\beta. \tag{3.12}$$

We would like to choose δ so that L_O and L_R are disjoint.

Overlap between L_O and L_R is possible only if $\beta_{l_1} = \beta'_{l_2}$ for some l_1, l_2. But $\beta_{l_1} = \beta'_{l_2}$ if and only if $l_1 + l_2 = -2\delta$ or, equivalently, if $2\delta \in \mathbb{Z}$. It follows that L_O and L_R are disjoint as long as $\delta \notin \{0, 1/2\}$.

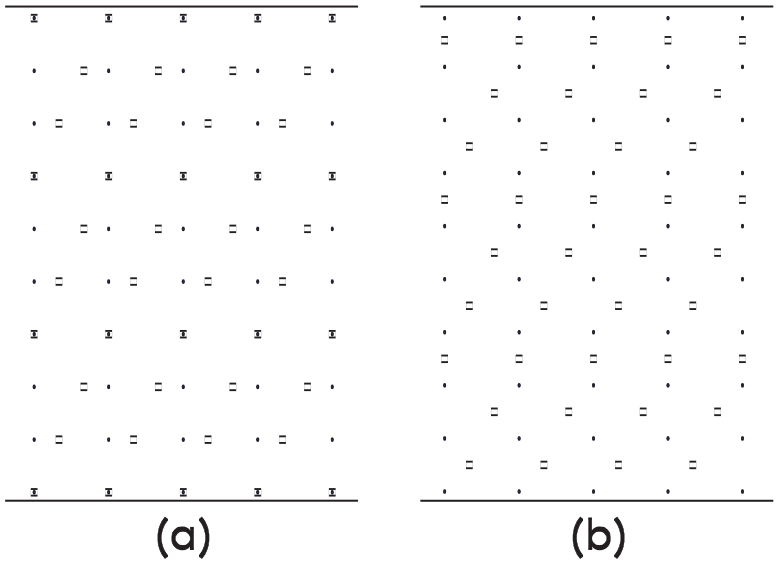

Figure 9: *The original lattice L_O (dots) and the reflected lattice L_R (squares) are both shown for $\Delta\alpha = 2\pi/4, \Delta\beta = \pi/6$. In (a) $\delta = 0$ and duplication occurs in every third row. In (b) $\delta = 1/4$ and L_R interlaces evenly with L_O.*

It is customary to use $\delta = 1/4$ as this interlaces the reflected sample points evenly with the original samples (see Figure 9). This so-called quarter detector shift is available, at least as an option, on all modern scanners [16].

With $\delta = 1/4$ we can reformulate L_R. From (3.3) we see that $\Delta\beta = \frac{p}{2q}\Delta\alpha$ and (3.12) becomes

$$\alpha'_{j,l} = \pi + \left(j + \left(l + \frac{1}{4}\right)\frac{p}{q}\right)\Delta\alpha, \qquad \beta'_l = -\left(l + \frac{1}{4}\right)\Delta\beta. \tag{3.13}$$

Note that the reflected points have undergone a shift of $\frac{1}{4}\Delta\beta$ in the β direction and a $\pi + \frac{p}{4q}\Delta\alpha$ shift in the α direction. Furthermore, a dynamic shift of $\frac{p}{q}\Delta\alpha$, which varies with l, is evident in the α direction.

Because of the dynamic shift $L_O \cup L_R$ cannot be generated by a single diagonal matrix. Thus, the sample points do not line up on a single rectangular lattice and we cannot use the standard reconstruction algorithm (Algorithm 5.3 in [17]). However, if we can recast $L_O \cup L_R$ as a union of shifted copies of a single rectangular lattice, then Faridani's multi-dimensional sampling theorem, Theorem 4, could be used.

4 Union of Rectangular Lattices

In this section we prove that the original lattice L_O and the reflected samples L_R can be seen as the union of several identical rectangular lattices, each shifted a fixed distance from the origin (see Theorem 5 of [4]).

Theorem 5. *Let* $\Delta\alpha = \frac{2\pi}{p}$ *and* $\Delta\beta = \frac{\pi}{q}$ *for some* $p, q \in \mathbb{Z}$. *Let*

$$L_O = \{(\alpha_j, \beta_l) : j, l \in \mathbb{Z}\},$$

$$\alpha_j = j\Delta\alpha, \qquad \beta_l = (l + \delta)\Delta\beta,$$

be an admissible sampling lattice arising from a quarter detector shift and let

$$L_R = \{(\alpha'_{j,l}, \beta'_l) : j, l \in \mathbb{Z}\},$$

$$\alpha'_{j,l} = \pi + \left(j + \left(l + \frac{1}{4}\right)\frac{p}{q}\right)\Delta\alpha, \qquad \beta'_l = -\left(l + \frac{1}{4}\right)\Delta\beta.$$

be the corresponding reflected sample points. Then $L_O \cup L_R$ *is a disjoint union of* $2q'$ *translates of the lattice*

$$L_P = \begin{pmatrix} \Delta\alpha & 0 \\ 0 & q'\Delta\beta \end{pmatrix} \mathbb{Z}^2, \tag{4.1}$$

where q' *is the denominator when* p/q *is reduced to lowest terms. The* $2q'$ *translates* a_m *are given by*

$$a_m = \begin{pmatrix} 0 \\ (m + \frac{1}{4})\Delta\beta \end{pmatrix}, \qquad a_{m+q'} = \begin{pmatrix} \pi + (m + \frac{1}{4})\frac{p}{q}\Delta\alpha \\ -(m + \frac{1}{4})\Delta\beta \end{pmatrix} \tag{4.2}$$

for $m = 0, \ldots, q' - 1$.

Proof. Let L_O and L_R be as described and let p/q be expressed in lowest terms as p'/q'. That is,

$$p' = \frac{p}{\gcd(p, q)}, \qquad q' = \frac{q}{\gcd(p, q)}.$$

For each $l_0 \in \mathbb{Z}$ let

$$[l_0] = \{l \in \mathbb{Z} : l = l_0 + c\,q', c \in \mathbb{Z}\}$$

and

$$L_{l_0 R} = \{(\alpha'_{j,l}, \beta'_l) : l \in [l_0], j \in \mathbb{Z}\}.$$

Note that the $[l_0]$ are the q' distinct equivalence classes in the group $\mathbb{Z}/q'\mathbb{Z}$. The points in each L_{l_0R} are given by

$$\begin{aligned}\alpha'_{j,l} &= \pi + \left(j + \left(l + \frac{1}{4}\right)\frac{p}{q}\right)\Delta\alpha \\ &= \pi + \left(j + \left(l_0 + cq' + \frac{1}{4}\right)\frac{p}{q}\right)\Delta\alpha \\ &= \pi + \left(l_0 + \frac{1}{4}\right)\frac{p}{q}\Delta\alpha + \left(j + cq'\frac{p}{q}\right)\Delta\alpha \\ &= \pi + \left(l_0 + \frac{1}{4}\right)\frac{p}{q}\Delta\alpha + j'\Delta\alpha\end{aligned}$$

for $j' = j + cp' \in \mathbb{Z}$, and

$$\begin{aligned}\beta'_l &= -\left(l + \frac{1}{4}\right)\Delta\beta \\ &= -\left(l_0 + cq' + \frac{1}{4}\right)\Delta\beta \\ &= -\left(l_0 + \frac{1}{4}\right)\Delta\beta - cq'\Delta\beta \\ &= -\left(l_0 + \frac{1}{4}\right)\Delta\beta - l'\Delta\beta\end{aligned}$$

with $l' = cq' \in \mathbb{Z}$. Thus, for each $l_0 \in \mathbb{Z}$ we can write the set L_{l_0R} as

$$\begin{aligned}L_{l_0R} &= \begin{pmatrix}\pi + \left(l_0 + \frac{1}{4}\right)\frac{p}{q}\Delta\alpha \\ -\left(l_0 + \frac{1}{4}\right)\Delta\beta\end{pmatrix} + \begin{pmatrix}\Delta\alpha & 0 \\ 0 & q'\Delta\beta\end{pmatrix}\mathbb{Z}^2 \\ &= \begin{pmatrix}\pi + \left(l_0 + \frac{1}{4}\right)\frac{p}{q}\Delta\alpha \\ -\left(l_0 + \frac{1}{4}\right)\Delta\beta\end{pmatrix} + L_P.\end{aligned}$$

Since a distinct lattice is obtained for each equivalence class $[l_0]$, we have that L_R is the disjoint union of the q' distinct L_{l_0R}. In other words,

$$L_R = \bigcup_{[l_0] \in \mathbb{Z}/q'\mathbb{Z}} L_{l_0R}. \tag{4.3}$$

Turning our attention to the original lattice L_O we see that for each l_0 the sample points are given by

$$\alpha_j = j\Delta\alpha,$$

with $j \in \mathbb{Z}$, and

$$\begin{aligned}\beta_l &= \left(l + \frac{1}{4}\right)\Delta\beta \\ &= \left(l_0 + cq' + \frac{1}{4}\right)\Delta\beta \\ &= \left(l_0 + \frac{1}{4}\right)\Delta\beta + l'\Delta\beta\end{aligned}$$

where $l' = cq' \in \mathbb{Z}$. Thus,

$$L_O = \bigcup_{[l_0] \in \mathbb{Z}/q'\mathbb{Z}} \begin{pmatrix} 0 \\ \left(l_0 + \frac{1}{4}\right)\Delta\beta \end{pmatrix} + L_P. \tag{4.4}$$

Combining (4.3) and (4.4) completes the proof. □

Note that when $q' = 1$

$$L_O \cup L_R = (L_P + a_1) \cup (L_P + a_2) \tag{4.5}$$

where

$$L_P = \begin{pmatrix} \Delta\alpha & 0 \\ 0 & \Delta\beta \end{pmatrix} \mathbb{Z}^2, \tag{4.6}$$

$$a_1 = \begin{pmatrix} 0 \\ \frac{1}{4}\Delta\beta \end{pmatrix}, \qquad a_2 = \begin{pmatrix} \pi + \frac{p}{2q}\Delta\alpha \\ -\frac{1}{4}\Delta\beta \end{pmatrix}. \tag{4.7}$$

We will return to this simple case later.

5 Application to Tomography

In this section we illustrate how Theorem 5 can be used together with Theorem 4 to reduce the number of measurements needed to obtain any resolution by half. We also discuss the third-generation problem and undertake a numerical experiment to verify our results.

5.1 The Mathematical Problem

The goal in tomography is to produce an accurate image of the interior of an object from a finite number of views. Mathematically, the problem is to reconstruct f given measurements of Df on some lattice L_W.

Let $f \in \mathcal{S}(\mathbb{R}^2)$ have support $|x| \leq \rho$ and be essentially b-bandlimited. The fan beam transform of f, $Df(\alpha, \beta)$, is periodic in both variables and can be viewed as a function on the group T^2. To reconstruct f with a resolution of

$2\pi/b$, the standard algorithm (Algorithm 5.3 in [17]) would require the standard lattice

$$L_W = \begin{pmatrix} \Delta\alpha & 0 \\ 0 & \Delta\beta \end{pmatrix} \mathbb{Z}^2$$

to satisfy the sampling conditions

$$\Delta\alpha = \frac{2\pi}{p} \leq \frac{r+\rho}{\rho}\frac{\pi}{br}, \qquad \Delta\beta = \frac{\pi}{q} \leq \frac{\pi}{br}. \tag{5.1}$$

Otherwise the reconstructed image will indicate structures which are not actually there. These so-called artifacts severely limit our ability to extract accurate information from the image.

Rather than sampling on L_W, suppose samples were taken on a lattice L_O, arising from a $\delta = 1/4$ detector shift, which was half as dense as L_W in the β direction. That is,

$$L_O = \begin{pmatrix} \Delta\alpha & 0 \\ 0 & \Delta\beta \end{pmatrix} \mathbb{Z}^2 + \begin{pmatrix} 0 \\ \frac{1}{4}\Delta\beta \end{pmatrix} \tag{5.2}$$

with

$$\Delta\alpha = \frac{2\pi}{p} \leq \frac{r+\rho}{\rho}\frac{\pi}{br}, \tag{5.3}$$

$$\Delta\beta = \frac{\pi}{q} \leq \frac{2\pi}{br}. \tag{5.4}$$

Clearly L_O does not satisfy the sampling conditions (5.1), so it cannot be used in the standard algorithm directly without creating serious artifacts.

We now describe a technique which will allow us to reconstruct f using L_O. First we employ Theorem 5 so that $L_O \cup L_R$ can be viewed as the union of shifted copies of L_P. Next we determine if the shifts a_m as given in (4.2) are such that the conditions of Theorem 4 are met. If so, we can compensate for the undersampling in β by using the interpolation formula (2.10). Since f is essentially b-bandlimited, (2.10) can be used to compute the missing samples with respect to L_W. After upsampling to the standard lattice L_W any reconstruction algorithm can be used. Since L_O is half as dense as L_W, we will have found a sampling scheme which requires half as many measurements as the standard scheme and is, in that sense, more efficient.

We will demonstrate this method in the simple case of $q' = 1$. With L_O as defined above (5.2), let L_R be the corresponding reflected lattice. Then, by Theorem 5

$$L_O \cup L_R = (L_P + a_1) \cup (L_P + a_2) \tag{5.5}$$

where

$$L_P = P\,\mathbb{Z}^2, \qquad P = \begin{pmatrix} \Delta\alpha & 0 \\ 0 & \Delta\beta \end{pmatrix}, \tag{5.6}$$

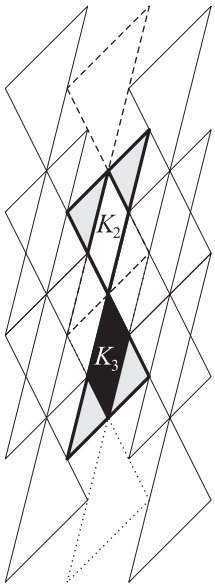

Figure 10: *Decomposition of the set K into mutually disjoint subsets K_1 (union of the gray sections), K_2 (white), and K_3 (black) by the translates $K-2\pi\left(P^{-1}\right)^T(0,0)^T$, $K-2\pi\left(P^{-1}\right)^T(0,-1)^T$, and $K-2\pi\left(P^{-1}\right)^T(0,1)^T$, respectively.*

$$a_1=\begin{pmatrix}0\\ \frac{1}{4}\Delta\beta\end{pmatrix},\qquad\qquad a_2=\begin{pmatrix}\pi+\frac{p}{2q}\Delta\alpha\\ -\frac{1}{4}\Delta\beta\end{pmatrix}. \tag{5.7}$$

We will now work toward applying Theorem 4.

The essential support of $\widehat{Df}$ is the set K specified in (3.2). Figure 10 shows K and some of the translates $K-2\pi\left(P^{-1}\right)^T k$, $k\in\mathbb{Z}^2$. If we decompose K into the mutually disjoint subsets K_1, K_2, and K_3 as indicated in Figure 10, we obtain $m_1=1$, $m_2=m_3=2$, hence $m=2$ and $L=3$. We also have

$$\begin{aligned}M_1&=\{k_1=(0,0)^T\}\\ M_2&=\{k_1,\ k_2=(0,-1)^T\}\\ M_3&=\{k_1,\ k_3=(0,1)^T\}.\end{aligned}$$

All that remains is to show that a_1,a_2 make the system (2.6, 2.7) solvable.

With a_1,a_2 as in (5.7), we find that

$$\begin{aligned}e^{-2\pi i\langle P^{-1}a_1,\,k_2\rangle}&=e^{-2\pi i\langle P^{-1}a_2,\,k_2\rangle}=e^{-\frac{\pi}{2}i}=-i,\\ e^{-2\pi i\langle P^{-1}a_1,\,k_3\rangle}&=e^{-2\pi i\langle P^{-1}a_2,\,k_3\rangle}=e^{\frac{\pi}{2}i}=i,\end{aligned}$$

and the system (2.6, 2.7) simplifies to

$$\begin{aligned} b_1^1 + b_2^1 &= 1 \\ b_1^2 + b_2^2 &= 1 \qquad & b_1^2 - b_2^2 &= 0 \\ b_1^3 + b_2^3 &= 1 \qquad & b_1^3 - b_2^3 &= 0. \end{aligned}$$

But this is easily solved by $b_1^2 = b_2^2 = b_1^3 = b_2^3 = \frac{1}{2}$ and any b_1^1, b_2^1 for which $b_1^1 + b_2^1 = 1$.

Applying Theorem 4 yields

Theorem 6. *Let $f \in \mathcal{S}(\mathbb{R}^2)$ be essentially b-bandlimited and have support in the disk of radius ρ with $0 < \rho < r$ for some $\rho, r \in \mathbb{R}$. Let*

$$K = \{(s,t) \in \mathbb{Z}^2 : |s-t| < br, |s|r < |s-t|\rho\}$$

denote the essential support of $\widehat{Df}$ and let

$$P = \begin{pmatrix} \Delta\alpha & 0 \\ 0 & \Delta\beta \end{pmatrix},$$

$$a_1 = \begin{pmatrix} 0 \\ \frac{1}{4}\Delta\beta \end{pmatrix}, \qquad a_2 = \begin{pmatrix} \pi + \frac{p}{2q}\Delta\alpha \\ -\frac{1}{4}\Delta\beta \end{pmatrix},$$

where

$$\Delta\alpha = \frac{2\pi}{p} \leq \frac{r+\rho}{\rho}\frac{\pi}{br}, \qquad \Delta\beta = \frac{\pi}{q} \leq \frac{2\pi}{br}.$$

for some $p, q \in \mathbb{Z}$ with $q' = q/gcd(p,q) = 1$. In addition, let $b_j^l = 1/2$ for $j = 1, 2$ and $l = 1, 2, 3$.

Then

$$|S_P Df(\alpha,\beta) - Df(\alpha,\beta)| \leq \frac{2}{\pi}\int_{\mathbb{Z}^2 \setminus K} |(Df)^\wedge(\xi)| d\xi, \tag{5.8}$$

where

$$S_P Df(x) = \frac{\pi(1+r)}{2b^2r^2}\sum_{j=1}^{2}\sum_{k \in A_P} Df(a_r + Pk)\widetilde{\chi}_{K_l}(x - a_r - Pk). \tag{5.9}$$

Since f is essentially b-bandlimited the right hand side of (5.8) is small (see [18]) and (5.9) can be used to accurately interpolate values of $Df(\alpha,\beta)$. After computing the missing β samples the standard reconstruction algorithm could be implemented.

Thus, Theorem 6 is a concrete example of the combined power of Theorems 4 and 5. If they can both be applied then, for any given bandwidth b, the amount of data needed for accurate reconstruction can be essentially cut in half. Consequently, we can double the resolution by doubling just the α density.

It is also possible to develop a reconstruction algorithm using L_P directly as was done by Izen et al. in [4]. However, that algorithm requires several additional restrictive hypotheses including shift-convexity of the bandregion K.

Roughly speaking, K is shift-convex if translates of K by non-zero elements of $L_W^\perp$ are disjoint and if additional shifts by elements of $L_P^\perp$ do not overlap K (see Definition 2.7 in [4]). Two examples are found in Figures 14,15 and discussed in Section 5.5. Note that this is more restrictive than the hypothesis of the Petersen-Middleton theorem, Theorem 2, which only requires that the translates $K + \eta$, $\eta \in L_W^\perp$ be disjoint. In contrast, Theorem 4 permits a finite number of overlaps.

5.2 The Third-Generation Problem

Since one of the major reasons for the work of Izen et al. was to overcome the third-generation problem, we feel compelled to discuss how this could be done.

In a third-generation CT scanner the x-ray source and detector array are mounted on a common rotating frame. When scanning, the source continuously fires an uninterrupted fan of x-rays and, at discrete time intervals, the detectors measure and record the strength of the beams. Increasing or decreasing the number of source locations is accomplished by shortening or lengthening the time between measurements. Thus, reducing the number of measurements does not reduce the amount of radiation and has no real medical or diagnostic benefits, though it may ease the computational burden.

The true diagnostic advantage comes from being able to take the available data and reconstruct an image whose resolution is higher than what is normally possible.

The maximum attainable resolution, for most third-generation scanners, is set by the spacing $\Delta\beta$ between detectors. Since the detector array is a contiguous collection of detectors, the detector spacing $\Delta\beta$ is also the detector width. This implies a maximum sampling-determined bandwidth of $b = \pi/\Delta\beta$ in the $\Delta\beta$ direction. Recalling that a b-bandlimited function cannot represent details smaller than $2\pi/b$, we see that only details larger than $2\Delta\beta$ are visible.

On the other hand, the mathematical model for the detector array suggests that the measured data is $2b = 2\pi/\Delta\beta$-bandlimited in the β direction[4]. To see this, suppose that each detector responds equally to all x-rays within $\Delta\beta/2$ of its center. Then the measured data $D'f$ is a convolution of Df with the detector response function. That is

$$\begin{aligned} D'f(\alpha,\beta) &= \frac{1}{\Delta\beta}\int_{-\Delta\beta/2}^{\Delta\beta/2} Df(\alpha,\beta-t)dt \\ &= \frac{1}{\Delta\beta} Df(\alpha,\beta) * \chi_{[-\Delta\beta/2,\,\Delta\beta/2]}. \end{aligned}$$

We know from our discussion in Section 1.1 that the essential bandwidth of $\chi_{[-\Delta\beta/2,\,\Delta\beta/2]}$ is $\frac{\pi}{\Delta\beta/2} = 2\pi/\Delta\beta$. Thus, the detectors are capable of measuring a cutoff frequency of $2b = 2\pi/\Delta\beta$ but their placement in the detector array reduces that frequency to $b = \pi/\Delta\beta$. The question of how to reconstruct at the higher hardware-determined bandwidth $2b$ is what constitutes the third-generation problem.

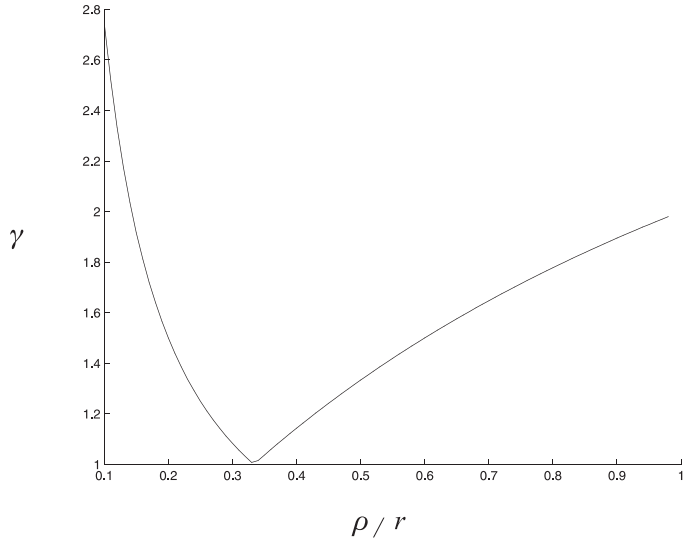

Figure 11: *The oversampling factor γ (5.12) caused by the condition $q' = 1$ in Theorem 6. Note that $\gamma = 1$ when $\rho/r = 1/3$ so there is no oversampling.*

Our solution is to follow the technique outlined in Section 5.1. A doubly fine sample is taken in the α direction, Theorem 5 is used to generate the matrix P and the shifts a_m and then, provided all of the conditions are met, Theorem 4 allows us to compensate for the undersampling in β. This will permit reconstruction at the maximum resolution consistent with the characteristics of the detector.

5.3 Oversampling

In Theorem 6 we asked that $q' = 1$ or, equivalently, that p be a positive integer multiple of q. This simplification can force us to oversample, or take more data than than the sampling conditions require. In this subsection we explain the causes and the extent of the oversampling in Theorem 6.

Third-generation scanners have a fixed number of detectors, so q and $\Delta\beta$ are predetermined. The source radius r and the scan radius ρ are also set by the physical geometry of the scanner. Thus, the sampling-determined bandwidth b is fixed. We assume that the scanner has been constructed so that

$$\Delta\beta = \frac{\pi}{q} \leq \frac{\pi}{br}. \tag{5.10}$$

The only parameter that we can choose somewhat freely is the number p of source locations. However, to reconstruct with a bandwidth of $2b$, p needs to

be chosen so that the sampling condition

$$\Delta\alpha = \frac{2\pi}{p} \leq \frac{r+\rho}{\rho}\,\frac{\pi}{2br} \tag{5.11}$$

is met.

Optimal sampling occurs when there is equality in (5.10),(5.11) and we let

$$p_o = \frac{4br\rho}{r+\rho}, \qquad\qquad q_o = br,$$

denote the optimal values of p and q. Whenever we use a p or q larger than the optimal value we we oversample by a factor of γ. It is desirable to make this as close to 1 as possible.

If $q' = 1$ then we must also make sure that p is an integer multiple of q. This additional constraint will be the cause of the oversampling.

One way to ensure that $q' = 1$ is to set $\rho/r = 1/3$. Many medical CT scanners are designed with $\rho/r \leq 1/3$ and $\rho/r \leq 1/2$ almost always. Note that $0 < \rho/r < 1$ since $0 < \rho < r$. If $\rho/r = 1/3$ then

$$\frac{p_o}{q_o} = \frac{4\rho}{r+\rho} = \frac{4\rho/r}{1+\rho/r} = 1,$$

and $q' = 1$. Thus, when $\rho/r = 1/3$ no oversampling is necessary–the optimal values satisfy both the sampling condition and the condition on q'.

When $\rho/r < 1/3$, the optimal value of p is less than the optimal value for q. To make $q' = 1$ we need to use $p = q_o$ instead of $p = p_o$. Thus, we are forced to take $\gamma = \frac{p}{p_o} = \frac{1+\rho/r}{4\rho/r}$ times more measurements than what the sampling conditions require.

If ρ/r is just slightly larger than $1/3$ then $p_o > q_o$. If we accepted the fact that q was fixed then the oversampling would jump suddenly on account of the stipulation that $p/q \in \mathbb{Z}^+$. However, designers of the scanner would undoubtedly know the ratio ρ/r and would instead choose to slightly increase q by taking $q = p_o$. This results in an oversampling factor of $\gamma = \frac{\frac{4br\rho}{r+\rho}}{br} = \frac{4\rho}{r+\rho}$.

Thus, when $q' = 1$, the oversampling factor γ is given by

$$\gamma = \begin{cases} \frac{1+\rho/r}{4\rho/r} & \text{if } 0 < \rho/r \leq 1/3, \\ \frac{4\rho}{r+\rho} & \text{if } 1/3 < \rho/r < 1. \end{cases} \tag{5.12}$$

The graph of γ is found in Figure 11.

5.4 Numerical Results

The results of Section 5.1 suggest that it is possible to reconstruct an image with the same resolution as the standard reconstruction algorithm but with just half of the data or, equivalently, double the resolution with just twice the data.

To confirm these findings we generate data for the phantom found in [4] which models a disk of water with two small pins of bone. This phantom was

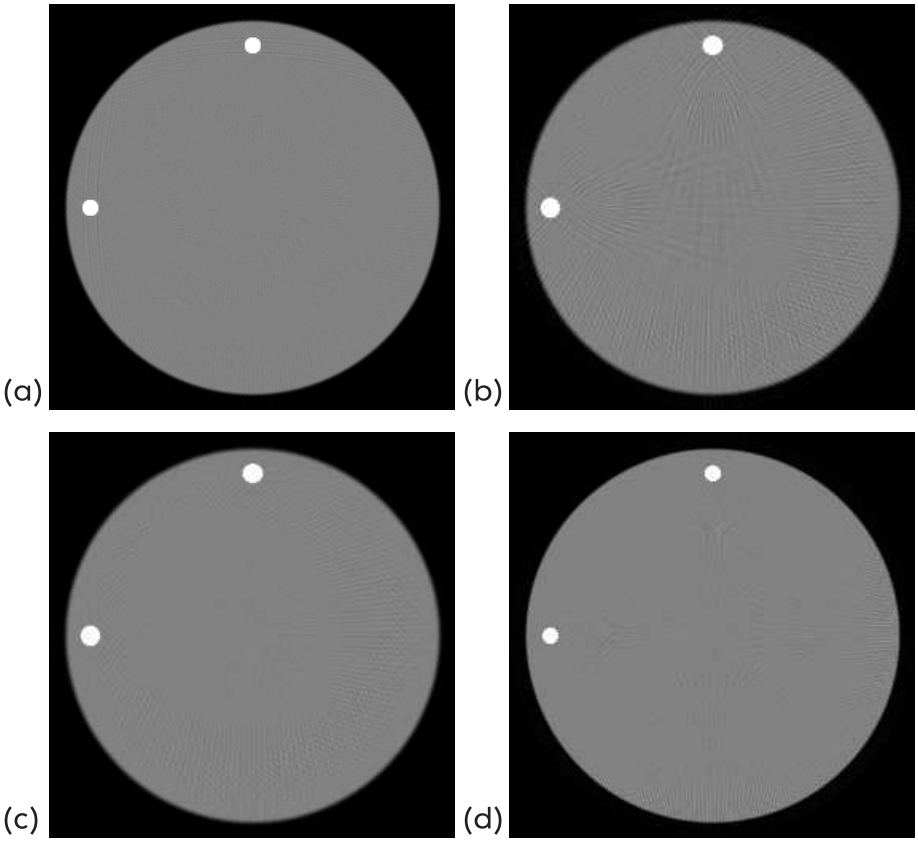

Figure 12: *Periodic reconstruction (a) with* $p = 600, q = 600$ *has twice the resolution as the standard reconstruction in (b) where* $p = 300, q = 600, b = 200$*. (c) uses the same data as (a) but in the standard algorithm and is no improvement over (b). (d) is comparable to (a) but needs* $p = 600, q = 1200$*.*

selected to test the scheme's ability to recover details near the edge of the scan circle. We use a source radius of $r = 3$ and scan radius $\rho = 1$ with a simulated bandwidth of $b = 200$.

To reconstruct with a bandwidth of $2b = 400$ we let $p = 600$, $q = 600$. Then, since we know $q' = 1$, we use Theorem 6 to interpolate the missing data and reconstruct with the standard algorithm (Algorithm 5.3 in [17]). The result is seen in Figure 12a.

If our scanner only had $q = 600$ samples available in β then it would be impossible to implement Algorithm 5.3 in [17] with $2b = 400$ directly since the sampling conditions (5.1) require $p \geq \frac{4br\rho}{r+\rho} = 600$ and $q \geq 2br = 1200$. The highest possible resolution would corresponding to a bandwidth of $b = 200$ with $p \geq 300, q = 600$ (see Figure 12b).

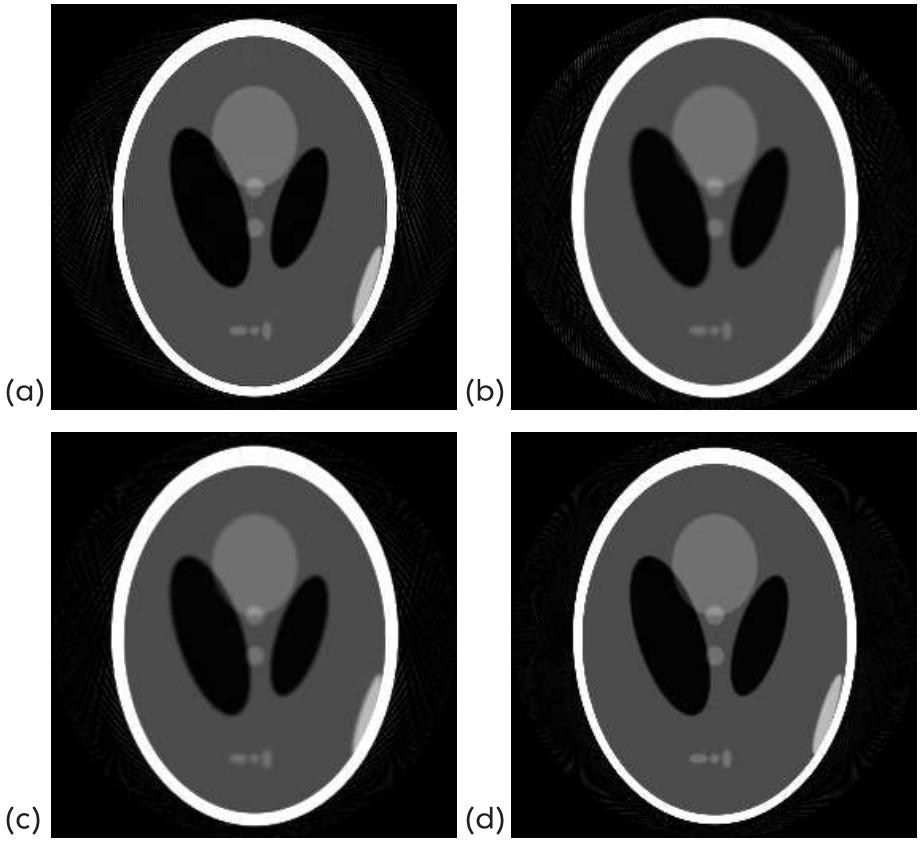

Figure 13: *Periodic reconstruction (a) of the Shepp-Logan phantom has twice the detail of the standard reconstruction in (b) but just twice the data. (c) has the data of (a) but the detail of (b). (d) matches the resolution of (a) but needs four times the data of (b).*

Thus, without the combination of Theorems 4 and 5, a third-generation scanner would be unable to achieve the detail of Figure 12a but would be limited to the resolution seen in Figure 12b.

Increasing p to 600 in the standard algorithm does little to improve the resolution, as can be seen in Figure 12c. It only serves to oversample by a factor of 2 in the α direction.

To apply the standard algorithm at a bandwidth of $2b = 400$ we would need $q = 1200$ β samples and $p = 600$ α samples (see Figure 12d). While this image has the same level of detail as Figure 12a, it requires twice the data.

The experiment was repeated for the Shepp-Logan head phantom [22] using the same p, q, b values as above. The reconstructed images are found in Figure 13 and verify the results obtained with the other phantom. This substantiates the

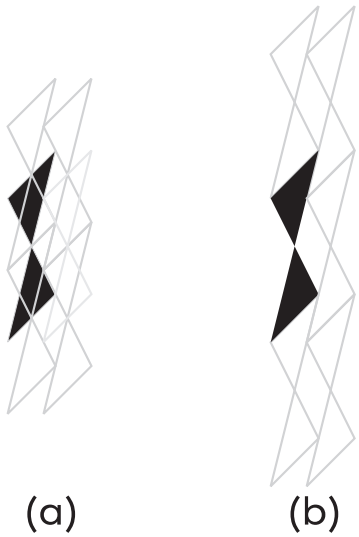

Figure 14: *The essential bandregion K of Df, solid, is shown with some of the translates $K + \eta, \eta \in L_W^\perp$. In (a) K is not shift-convex since the translates overlap K. This is not the case in (b) where K is shift-convex. In both $L_W^\perp = W^\perp\mathbb{Z}^2$ where $W^\perp$ is defined by (5.13) in (a) and by (5.15) in (b).*

theory of [4] and illustrates the practical application of Theorem 6.

5.5 A Few Words On Shift-Convexity

The reconstruction algorithm presented [4] (Algorithm 3.2) requires the essential bandregion K to be shift-convex. In neither of the examples in Section 5.4 was K shift-convex. With $\rho/r = 1/3$ and equality in (5.11,5.10) we have

$$W = \begin{pmatrix} \frac{r+\rho}{\rho}\frac{\pi}{2br} & 0 \\ 0 & \frac{\pi}{br} \end{pmatrix}, \qquad W^\perp = \begin{pmatrix} \frac{4br\rho}{r+\rho} & 0 \\ 0 & 2br \end{pmatrix}. \tag{5.13}$$

As can be seen in Figure 14a, both $K + W^\perp(0,1)^T$ and $K + W^\perp(0,-1)$ overlap K which, by replacing b by $2b$ in (3.2, is given by

$$K = \{(s,t) \in \mathbb{Z}^2 : |s-t| < 2br, |s|r < |s-t|\rho\}. \tag{5.14}$$

To make K shift-convex we would need to have chosen

$$W = \begin{pmatrix} \frac{r+\rho}{\rho}\frac{\pi}{2br} & 0 \\ 0 & \frac{\pi}{2br} \end{pmatrix} \qquad W^\perp = \begin{pmatrix} \frac{4br\rho}{r+\rho} & 0 \\ 0 & 4br \end{pmatrix}, \tag{5.15}$$

as is done in [4] (see section 3.2.2). A few of the translates $K + \eta, \eta \in L_W^\perp$ are in Figure 14b.

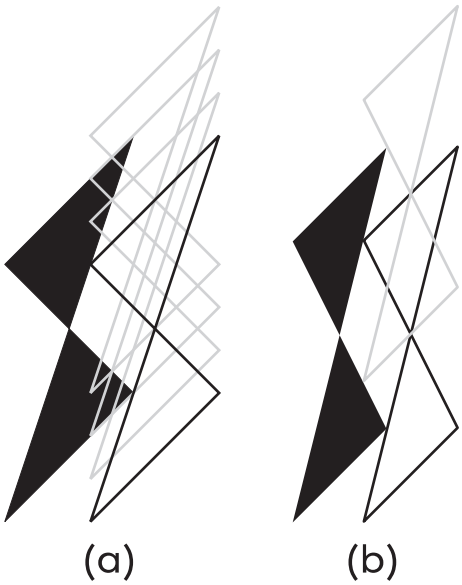

Figure 15: *The reconstruction algorithm of Izen et. al (Algorithm 3.2 in [4]) requires the essential bandregion K of Df, solid, to be shift convex with respect to $L_W^\perp$ and $L_P^\perp$. Translates by $L_W^\perp$ are in black while shifts by $L_P^\perp$ are gray. In (a) the translates $K+\eta, \eta \in L_W^\perp$ do not overlap K but additional shifts by elements of $L_P^\perp$ reintroduce overlap,. Such is not the case in (b) where K is shift-convex. Both figures are drawn with W and P as in (5.15) and (5.16). (a) corresponds to $\rho/r = 1/2$ and in (b) $\rho/r = 1/3$.*

As was mentioned earlier, a bandregion K can fail to be shift-convex even when $K \cap (K+\eta) = \emptyset$ for all $\eta \in L_W{}^\perp$. This happens when additional shifting by elements of $L_P^\perp$ causes overlap with K. As an example, let $\rho/r = 1/2$ with equality in (5.11,5.10). Take W and $W^\perp$ as in (5.15) and

$$P = \begin{pmatrix} \frac{r+\rho}{\rho} & \frac{\pi}{2br} \\ 0 & \frac{\pi q'}{br} \end{pmatrix}, \qquad P^\perp = \begin{pmatrix} \frac{4br\rho}{r+\rho} & 0 \\ 0 & \frac{2br}{q'} \end{pmatrix}. \tag{5.16}$$

Since $\rho/r = 1/2,\ p/q = 4/3$ so $q' = 3$. Then $K \cap (K + W^\perp(1,0)^T + P^\perp(0,1)^T) \neq \emptyset$ as can be seen in Figure 15a. Several multiples of $P^\perp(0,1)^T$ also reintroduce overlap. However, K is shift convex with respect to $L_W^\perp$ and $L_P^\perp$ if we use (5.15) and (5.16) with $\rho/r = 1/3$ (see Figure 15b).

We conclude this section with a reconstruction of both phantoms for a decidedly non-shift-convex bandregion K. This is done simply to illustrate the flexibility of combining Theorems 5 and 4. With, $\rho/r = 1/2$, equality in (5.11,5.10), and W, P as in (5.13),(5.16), overlap occurs both with shifts from $L_W^\perp$ and with additional shifts from $L_P^\perp$. We chose $b = 400$ so that the images could be compared with the earlier reconstructions. With equality (5.11,5.10) we have

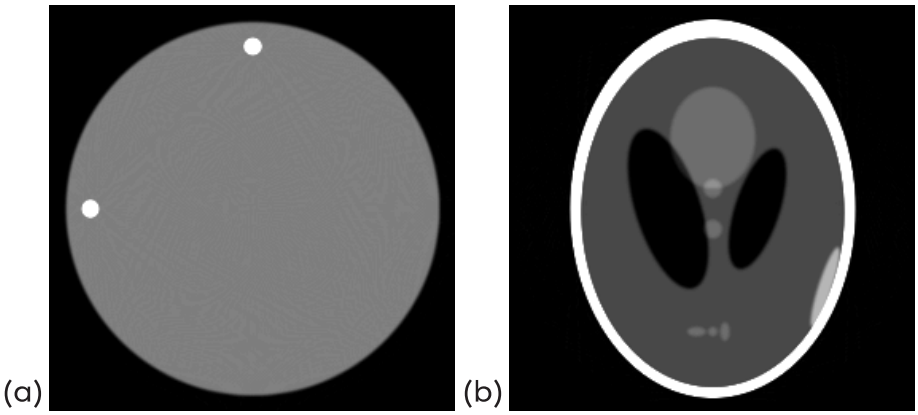

Figure 16: *Reconstruction of two phantoms with* $\rho/r = 1/2$ *and bandwidth* $b = 400$. *With* $\rho/r = 1/2$ *the essential bandregion* K *is as in Figure 15b and is not shift-convex, and Algorithm 3.2 in [4] would be unable to produce this image.*

$p = 1067$ and $q = 800$. The upsampling, as in the earlier reconstructions, was performed by Faridani's PSMD software package and the reconstruction followed Algorithm 5.3 in [17]. Figure 16 shows the results.

6 Conclusions

We have verified the results of Izen et al. in [4] and have avoided the restrictive hypothesis of shift convexity by employing Faridani's periodic multi-dimensional sampling theory, Theorem 4. The results showed that the number of data needed for accurate reconstruction in the fan beam geometry can be effectively cut in half.

This led to the presentation of a new scheme which is more efficient than standard reconstruction and is easier to implement than the efficient scheme of Natterer [15]. It also provided an answer to the undersampling inherent in the design of third-generation CT scanners, permitting reconstruction at the maximum possible. The validity of the theory was demonstrated through a numerical implementation of Theorem 6.

Theorem 6 is not intended to be the only possible application of Theorems 4 and 5, but simply a concrete example of their combined power. As we saw in Figure 16, the PSMD software package developed by Faridani in conjunction with [7] permits interpolation regardless of the value of q'.

6.1 Acknowledgment

I would like to thank Dr. Adel Faridani for his valuable insights and advice and for the use of his software package for multi-dimensional periodic sampling.

References

[1] R. N. Bracewell, *The Fourier Transform and Its Applications*, Second Edition, McGraw-Hill, 1986.

[2] S. R. Deans, *The Radon transform and some of its applications*, Wiley, New York, NY, 1983.

[3] S. H. Izen, *Generalized Sampling Expansion on Lattices*, IEEE Trans. Signal Processing, to appear.

[4] S. H. Izen, D. P. Rohler, and K.L.A. Sastry, *Exploiting Symmetry in Fan Beam CT: Overcoming Third Generation Undersampling*, SIAM J. Appl. Math., 65 (2005), pp. 1027-1052.

[5] A. Faridani, *An application of a multidimensional sampling theorem to computed tomography*, in [11], pp 65-80.

[6] A. Faridani, *Reconstructing from efficiently sampled data in parallel-beam computed tomography*, in G.F. Roach (ed.), Inverse problems and Imaging, Pitman Research Notes in Mathematics Series, Vol. 245, Longman Press, London, 1991, pp. 68-102.

[7] A. Faridani, *A generalized sampling theorem for locally compact abelian groups*, Math. Comp., 63 (1994), pp. 307-327.

[8] A. Faridani, *Sampling in parallel-beam tomography*, in Inverse Problems and Imaging, A.G. Ramm (ed.), Plenum, New York, NY, 1998, pp. 33-53.

[9] A. Faridani and E. L. Ritman, *High-resolution computed tomography from efficient sampling*, Inverse Problems, 16 (2000), pp. 635-650.

[10] A. Faridani, *Introduction to the mathematics of computed tomography*, Inside Out: Inverse Problems and Applications, 2003, pp. 1-46.

[11] E. Grinberg and E. T. Quinto (eds.), *Integral Geometry and Tomography*, Contemporary Mathematics, Vol. 113, AMS, Providence, RI, 1990.

[12] H. Kruse, *Resolution of reconstruction methods in computerized tomography*, SIAM J. Sci. Stat. Comput, 10 (1989), pp 447-474.

[13] I. Kluvanek, *Sampling theorem in abstract harmonic analysis*, Mat. Casopis Sloven. Akad. Vied, 15 (1956), pp. 43-48.

[14] F. Natterer, *The Mathematics of Computerized Tomography*, Wiley, New York, NY, 1986.

[15] F. Natterer, *Sampling in fan-beam tomography*, SIAM J. Appl. Math., 53 (1993), pp. 358-380.

[16] F. Natterer, *Sampling Functions with Symmetries*, Preprint, `http://wwwmath.uni-muenster.de/math/inst/num/Preprints/1999-/natterer_1/paper.pdf` , 1998.

[17] F. Natterer and F. Wuebbeling, *Mathematical Methods in Image Reconstruction*, SIAM, Philadelphia, PA, 2001.

[18] V.P. Palamodov, *Localization of harmonic decomposition of the Radon transform*, Inverse Problems, 11 (1995), pp. 1025-1030.

[19] A. Papoulis, *Signal Analysis*, McGraw-Hill, 1977.

[20] D.P. Petersen and D. Middleton, *Sampling and reconstruction of wave-number-limited functions in N-dimensional euclidean space*, Inf. Control, 5 (1962), pp. 279-323.

[21] C.E. Shannon, *Communication in the presence of noise*, Proc. IRE, 37 (1949), pp. 10-21.

[22] L. Shepp and B. Logan, *The Fourier Reconstruction of a Head Section*, IEEE Trans. Nuclear Science, NS-21 (1974), pp.21-43

[23] Siemens Medical Solutions, *Personal correspondence with LuJean Smith*, July 2004.

[24] K.T. Smith, D.C. Solmon, and S.L. Wagner, *Practical and mathematical aspects of the problem of reconstructing objects from radiographs*, Bull. Amer. Math. Soc., 73 (1977), pp.1227-1270.

[25] E.M. Stein and G. Weiss, *Introduction to Fourier Analysis on Euclidean Spaces*, Princeton University Press, Princeton, NJ, 1971.

[26] K. Yosida, *Functional Analysis*, Fourth Edition, Springer-Verlag, New York, NY, 1974.